Journal of Ovonic Research Vol. 14, No. 1, January - February 2018, p. 17 - 25

RESPONSIVITY ENHANCEMENT OF LUTETIUM OXIDE DOPED –NiO THIN FILMS

I. M. IBRAHIM[a], A. S. MOHAMMED[b,d], A. RAMIZY[b,c]
aDepartment of Physics, college of Science, University of Baghdad, Baghdad,iraq
bDepartment of Physics,College of Science,University of Anbar, Anbar, Iraq
cRenewable energy Research Center, University of Anbar, Anbar, Iraq
dMinistry of Education, Direction of Education in AL-Anbar

Metal oxide nanoparticles doped with rare earth lutetium oxide (Lu_2O_3) at 0%, 2%, 4%, and 6% are deposited on porous silicon (PS) substrates by pulsed laser deposition (PLD) technique for the manufacture of ultraviolet (UV) detector. An electrochemical etching process (ECE) is then performed to fabricate porous silicon (PS), which uses a substrate n-type Si with orientation <111>, at an etching current of 15 mA/cm^2 and constant etching time of 20 min. Meanwhile, the nickel oxide (NiO)films with doping ratio of Lu_2O_3 have polycrystalline cubic structures, as indicated by the X-ray diffraction patterns of the films.Result shows that the mean crystallite size of NiO decreases with increasing doping ratio. The direct energy gap (E_g) of NiO is 3.4 eV and increases with increasing doping ratio. UV detector is fabricated using Au/NiO:Lu_2O_3/PS at a ratio of 2% and 6%, respectively. The sample doped with 6% lutetium exhibit good sensitivity approximately 126% .

(Received October 8, 2017; Accepted January 5, 2018)

*Keywords:*Metal oxide; Rare earth, Porous silicon;Pulsed-laser deposition

1. Introduction

Nanostructured transparent conducting oxides (TCOs) have been extensively studied because of scientific interest and their potential applications. TCO films, such as tin oxide, zinc oxide, cadmium oxide, and indium tin oxide are used in window coatings and transparent electrodes. All these TCO are n-type. Meanwhile, p-type TCO thin films are used in several applications, such as transparent electrodes for optoelectronic devices, which are used for hole injection. Nickel oxide (NiO) is one of the most important antiferromagnetic p-type semiconductors [1].NiO exhibits a wide band gap energy within the UV region in the range of 3.5–4.0eV at room temperature[2–3].These materials have attracted attention because of their excellent chemical stability, low cost, and promising storage properties [4–5]. Metal oxide NiO films are often used in counter electrodes, gas sensors, displays, LEDs, and variable reactance mirrors [6]. They are also used in catalysts, electrochromic devices, solar cells, battery cathodes, large span optical densities, full cells, and TCOs [7–9]. NiO thin films are prepared through different techniques, such as screen printing, spray pyrolysis, radio frequency magnetron sputtering, microwave, electron beam evaporation, and pulsed laser deposition (PLD) [10–16]. The PLD method is a versatile technique and is principally used because of the stoichiometric transfer between the target and deposition film. Therefore, this method has numerous advantages. In particular, it can efficiently control the composition of thin films to facilitate their rapid and effective growth process. It enables the deposition of different kinds of oxides, polymers, carbides, nitrides, and metallic systems [17]. Meanwhile, different kinds of the solid-state photo detectors (PDs) are prepared, such as metal–semiconductor–metals(MSMs), Schottky diodes, and p–n junction structures. PD-type MSMs have received special attention, because they can be fabricated

*Corresponding author: asmat_hadithi@uoanbar.edu.iq

easily and are flexible [18].The aim of this work is to investigate the influence of rare-earth Lu_2O_3 on the properties of NiO/PS. Nano films are prepared by the PLD method at room temperature. The structural and optical properties of thin films are controlled by changing rare earth concentration during film growth possessing.

2. Experimental setup

PS layers were formed through the electrochemical etching (ECE) of n-type <111> oriented silicon substrate at a resistance of 1–4 Ω. The ECE cell was made of Teflon (or any highly acid-resistant polymer). Si wafer was cut into square-shape pieces (1 cm^2) and then anodized in a solution containing 48% HF and ethanol at 1:4 ratio and current density of 15 mA/cm^2 for 20 min under illumination (70 W halogen lamp placed 20 cm from the sample). The Si wafers were ultrasonically cleaned in distilled water and acetone. A two-electrode setup is applied, and Si was used as anode and Pt mesh as cathode. As shown in Fig. 1, NiO powders at different doping concentrations of lutetium (Lu_2O_3) at 0, 2, 4, and 6 wt% were mixed using a gate mortar and then pressed under 5 t to form targets with 2 cm diameter and 0.2 cm thickness. The targets were ensured to be dense and homogeneous as possible to produce good quality Lu_2O_3:NiO thin films, which would be deposited by the PLD technique. Film deposition was carried out inside a 10^{-3}Torr evacuated vacuum chamber. The focused Q-switched Nd:YAG laser beam was incident at an angle of 45° on the target surface, and the energy of the laser was 500 mJ. The MSM device was fabricated by the metallization of samples, and the metal contacts of finger-shaped gold (Au) electrodes of 250 nm thickness were deposited on top of the NiO:Lu_2O_3/PS sample using an E306A Edwards thermal evaporation system. The film thickness was determined by Filmetrics (F20) and varied within 200 ± 5 nm. The structure properties, which included crystal structure and grain size, were analyzed by X-ray diffractometer system with a BRUKER (AXS), in which the source of radiation was Cu(kα) and the wavelength was 1.5406 Å. The morphology of the surfaces of the films was tested via (FESEM, JSM-7600F). The electrical properties of the developed PD were tested by Keithley Model 4200-SCS instrument and Fluke 8846A Multimeter.

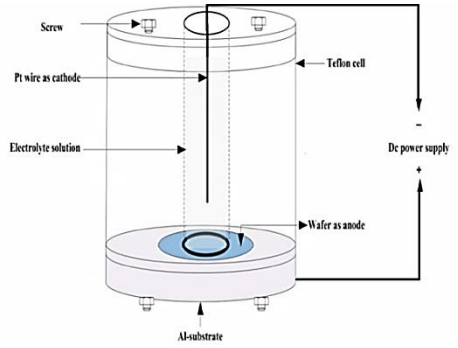

Fig. 1. Porous silicon fabrication setup [19]

3. Result and discussion

3.1 Structure

Fig. 2 shows the XRD scan of NiO thin film doped with rare earth Lu_2O_3 deposited on PS at RT substrate temperature illustrated in Fig. 1.The peak of pure Si is located at approximately 28.4° and related to (111) direction. XRD pattern shows that all doped and undoped films are polycrystalline. The XRD pattern exhibits numerous peaks at 2θ of 37.3 and 43.3, which are referred to (111) and (200) planes of the cubic structure of NiO, respectively, according to the JCPDS file (card no.96-900-8694). This result is in agreement with that of Sta [20]. The (111) peak has the highest intensity, indicating that (111) is the preferred orientation. In addition, many peaks referring to lutetium oxide at 2θ of 29.7, 34.5, and 49.6 are observed and refer to the (222),

(400), and (440) planes of the cubic structure of Lu_2O_3, respectively, from the International Center for Diffraction (card no. 96-101-0596). The increase in the intensity peak of NiO when doped with Lu_2O_3 at 2% concentration. Table (1) shows the experimental data of standard peaks. The Debye-Scherrer formula [21] is used to calculate the mean crystalline size from the FWHM of XRD lines.

$$D = \frac{K\lambda}{\beta cos\theta} \quad (1)$$

where K is the Scherrer constant which is usually equal to 0.9, β is FWHM in radians, λ is the wavelength in nanometers, and θ is the diffraction angle in radians. The result shows that the mean crystallite size of NiO decreases when doping ratio, and FWHM both increases, as shown in Table 1. This result indicates that the nanocrystalline are domains.

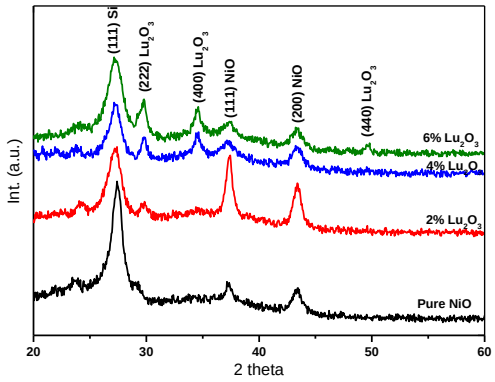

Fig. 2. X-ray diffraction patterns of Lu_2O_3-doped NiO films deposited on PS at doping ratios of 0, 2, 4, and 6 wt%.

Table 1. Structural parameters of Lu_2O_3-doped NiO films/porous Silicon deposited at different doping ratios(2, 4, and 6) wt%

Lu_2O_3%	2θ (Deg.)	FWHM (Deg.)	d_{hkl} Exp.(Å)	G.S (nm)	d_{hkl} Std.(Å)	hkl	Phase	card No.
0	27.4520	0.8818	3.2464	9.3	(111)	3.1414	Cub. Si	96-901-3105
	37.3200	0.6446	2.4076	13.0	(111)	2.4066	Cub. NiO	96-900-8694
	43.3800	0.9829	2.0842	8.7	(200)	2.0842	Cub. NiO	96-900-8694
2	27.3420	0.9340	3.2592	8.8	(111)	3.1414	Cub. Si	96-901-3105
	29.7840	0.7130	2.9973	11.5	(222)	2.9936	Cub.Lu_2O_3	96-101-0596
	37.3510	0.7430	2.4056	11.3	(111)	2.4066	Cub. NiO	96-900-8694
	43.3940	0.8210	2.0836	10.4	(200)	2.0842	Cub. NiO	96-900-8694
4	27.3240	0.9510	3.2613	8.6	(111)	3.1414	Cub. Si	96-901-3105
	29.7952	0.5420	2.9962	15.2	(222)	2.9936	Cub.Lu_2O_3	96-101-0596
	34.5437	0.6340	2.5944	13.1	(400)	2.5925	Cub.Lu_2O_3	96-101-0596
	37.3330	1.0320	2.4067	8.1	(111)	2.4066	Cub. NiO	96-900-8694
	43.3720	1.0610	2.0846	8.1	(200)	2.0842	Cub. NiO	96-900-8694
6	27.3310	1.3030	3.2605	6.3	(111)	3.1414	Cub. Si	96-901-3105
	29.8011	0.6540	2.9956	12.6	(222)	2.9936	Cub.Lu_2O_3	96-101-0596
	34.5410	0.7150	2.5946	11.6	(400)	2.5925	Cub.Lu_2O_3	96-101-0596
	37.3520	1.1160	2.4056	7.5	(111)	2.4066	Cub. NiO	96-900-8694
	43.3260	1.1180	2.0867	7.6	(200)	2.0842	Cub. NiO	96-900-8694
	49.6660	0.5420	1.8342	16.2	(440)	1.8332	Cub.Lu_2O_3	96-101-0596

3.2 Morphological properties

Fig. 3a shows the FESEM image of NiO/PS thin film obtained from Ni oxidized at room temperature, etching current of 15 mA, and etching time of 20 min. Notably, the image shows that the small nanoparticles observed include a number of particles with a grain size of 13 nm (XRD analysis). Spherical and condense particles are observed, and the white particles are metallic Ni particles randomly distributed on the black background. Fig. 3b and c show the FESEM images of NiO/PS doped Lu_2O_3 at 2% and 6% doping, respectively, in which the color of the particle gradually changed with less lighting. The surface became more homogeneous with more spherical and condensed particles, especially at the doping ratio of 6% lutetium which is embedded inside the NiO matrix with increased doping. In general, when the thickness of the films was 200 ± 5 nm, the pore size decreased with increasing doping ratio, because the pore size strongly depends on the shape of the crystallite size and grain boundaries of the thin films. Therefore, compared with the XRD result, the crystal size decreases when doping Lu_2O_3 ratio increases. Figures 4a, b, and c are cross-sections of NiO/PS, Lu_2O_3(2%):NiO/PS, and Lu_2O_3(6%):NiO/PS, respectively. The image shows the occurrence of nonparallel and partially cracked silicon walls, which result in asymmetrical and narrow holes between them. The image shows that the thickness of the film is approximately 200 ± 5 nm, and the thickness of porous is approximately 17 µm.

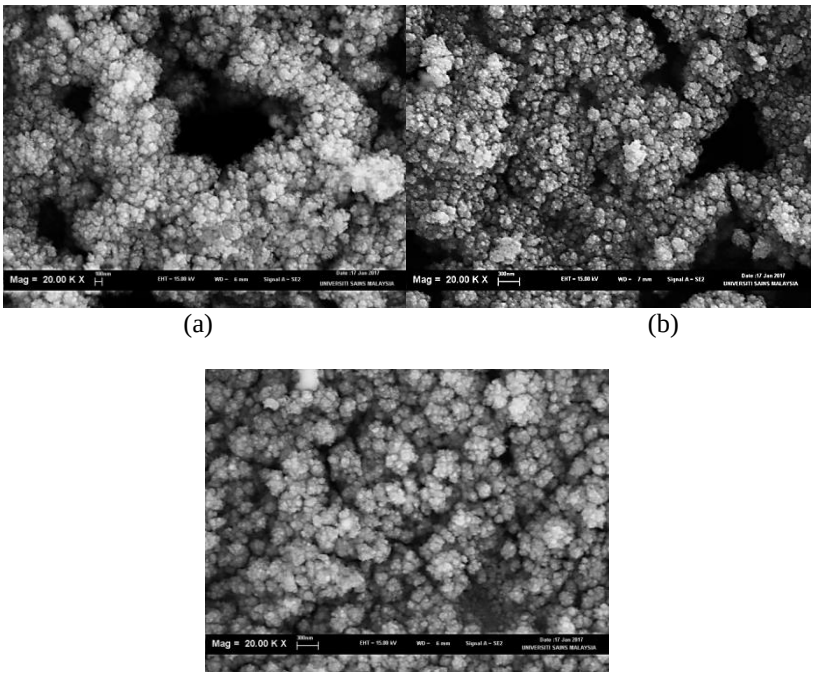

(a) (b)

(c)

Fig. 3. FESEM images of (a) NiO/PS, (b) NiO:Lu_2O_3/PS at 2%, and (c) NiO: Lu_2O_3/PS at 6%.

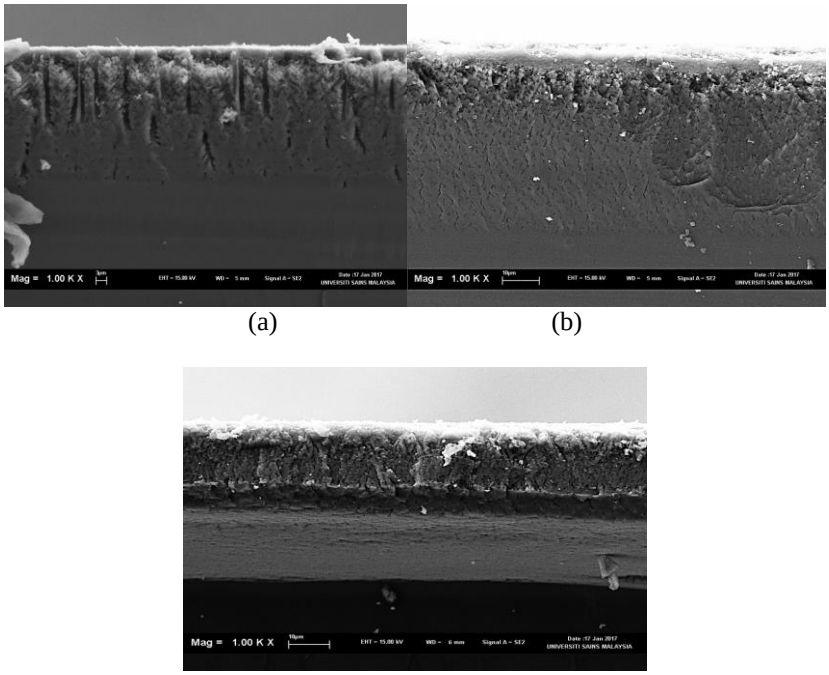

(a) (b)

(c)

Fig. 4. Cross-sections (a) NiO/PS, (b) NiO:Lu_2O_3/PS at 2%, and (c) NiO: Lu_2O_3/PS at 6%

Table 2: Ideality factor (β) and tunneling factor (At) of Au/NiO/PS, Au/NiO:Lu_2O_3/PS at 2%, and Au/NiO:Lu_2O_3/PS at 6%

Sample	Ideality Factor (β)	Tunneling Factor (At)
Pure NiO	1.117	2.077
Lu_2O_3 2%	1.6	2.45
$Lu_2O_3$6%	1.48	2.39

3.3 Optical properties

Optical energy gap can be used to estimate the difference in energy between the valence and conduction bands, which can help determine the thermoelectric and electronic properties of the materials. The direct energy gap (E_g) is determined by using Tauc formula, with relation to r = 1/2 yields linear dependence, that is, the optical band gap has directly allowed transition [22] The optical band gap of NiO films of undoped and doped lutetium is on a glass substrate as shown in Figure 5 from the plot of ($\alpha h\nu^2$) as a function of photon energy ($h\nu$). The optical band gap is estimated by extrapolating the linear portion to zero absorption coefficient ($\alpha = 0$).From figure 5, the energy band gap of NiO at a thickness of 200 nm is found to be notably 3.4 eV. Our result is in good agreement with Ahmed J. Hassan [11], in which NiO doping lutetium at 2%, 4%, and 6% increases the band gap energy to 3.5, 3.6, and 3.8 eV. This trend shifted toward high energy (red shift) as a result of the reduction of grain size [23]. Hence, compared with the XRD result, the crystal size decreased with the increase of doping Lu_2O_3 ratio. This result can be attributed to the quantum confinement effects which specifically occur in semiconductor nanoparticles. The small size of nanoparticles is responsible for different properties, such as optical, electronic, and electrical [24]. The effect of quantum confinement leads to the increase of the energy band whenever the particle size decreases due to the restriction of particle movement in one dimension. In addition, the FESEM image shows the doping with lutetium enhancement in the structure.

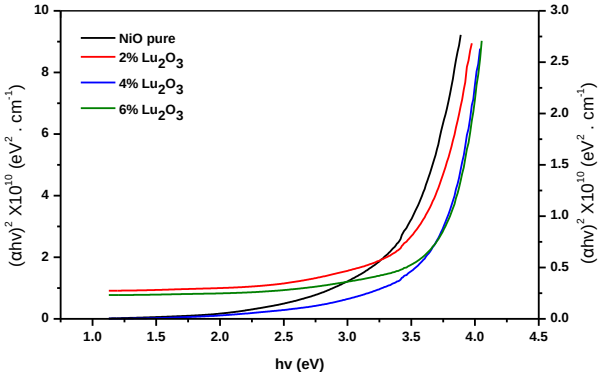

Fig. 5. Optical energy gap of NiO:Lu_2O_3 at (0, 2, 4, 6)%.

3.4 Current-Voltage Characteristics (I-V).

Fig. 6 show I–V characteristics in the dark for Au/NiO/PS heterojunction-doped Lutetium (Lu_2O_3) in the forward bias. The results exhibit that the current has two regions. The first region at a low voltage due to the recombination current, in which the generated concentration of the generated carriers is higher than the intrinsic carrier concentration. The second region is at a high voltage due to the diffusion current. In addition, two regions are located in the reverse bias. The first region is a low voltage bias, in which electron-hole pairs are generated due to the generated reverse current with increasing voltage. In the second region at a voltage higher than 0.5 V, the reverse current resulted from the diffusion of minority carriers through the junction, which caused major increases within the reverse bias [25]. The depletion layer in the semiconductor and the barrier on the interface are generated as a result of the Fermi level along the metal and semiconductor when they are in contact due to the charge motion from the higher energy toward the lower energy side [26]. Therefore, from the notable rectifying behavior of figure 6, the Schottky barrier at Au/NiO:Lu_2O_3/PS interface is achieved. The ideality factor (β) and the tunneling factor calculated from the forward bias are shown in table 3. The prepared sample exhibited good ideality factor for pure NiO and with doped Lu_2O_3 at 6%. This result is due to the diffusion current which controls at the interface while showing an increase in ideality factor (β) when doping Lu_2O_3 at 2%. This is attributed to the dominant recombination current [27]. The tunneling factor (At) decreased with the decrease of ideality factor.Figure7 shows the I–V characteristics of Au/NiO/PS doped lutetium (Lu_2O_3) planar system under ambient light illumination of100 mw/cm^2 and 183 mw/cm^2 as a function of varying doping concentrations. Figure 7 (a) shows that the I–V characteristics under light illumination of 100 mw/cm^2 for NiO/PS, Au/NiO:Lu_2O_3/PS at 2%, and Au/NiO:Lu_2O_3/PS at 6% respectively in the prepared sample of NiO/PS reveals a low current. This resulted in the high resistivity and Schottky barrier height of the proposed PD in comparison to other samples. Meanwhile, when doping lutetium, the sample of Lu_2O_3 at 2% and 6% showed that the electrical properties are improved due to the influence of rare earth ions which cause structural disorder and lattice strain, subsequently increasing the electrical properties[28]. Figure 7(b) shows the illumination at 183 mw/cm^2. When the intensity of lighting is 183 mw/cm^2, the prepared detector showed a high response to the intensity of the optical capacity. Meanwhile, in the case of reverse bias, the width of the depletion layer increases with the increase of the applied voltage. Thus, the incident radiation increased both equally working voltage on the twin separated electron-hole on both ends of the depletion layer, thereby contributing to the optical current.

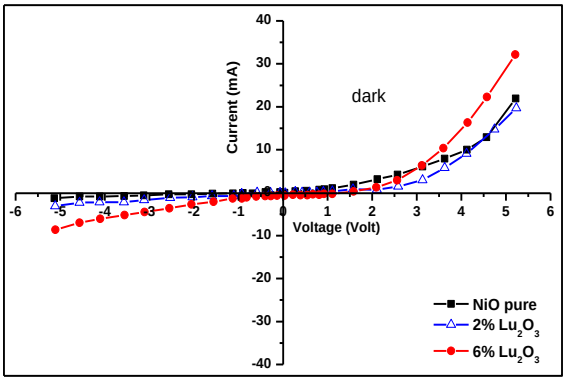

Fig. 6. I–V characteristic in dark for Au/NiO/PS, Au/NiO:Lu_2O_3/PS at 2%, and Au/NiO:Lu_2O_3/PS at 6%.

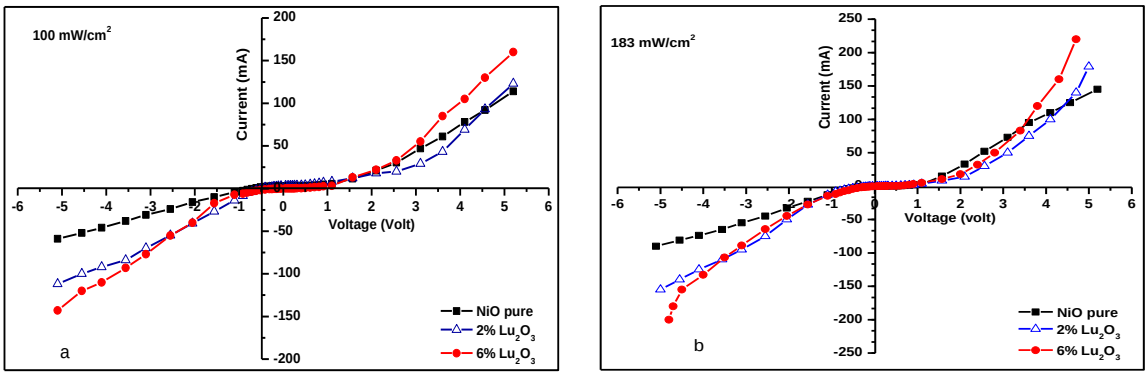

Fig. 7. I–V characteristic under illumination of Au/NiO:Lu_2O_3/PS at 2% and Au/NiO:Lu_2O_3/PS at 6% at (a) 100mw/cm^2 and (b) 183mw/cm^2

Table 3: Photoconductivity parameters of Au/ NiO/PS doped Lu_2O_3 at 2% and 6%.

Sample	Sensitivity(S)%	Rise Time(s)	Recovery Time(s)
Pure NiO	66	0.800	0.800
Lu 2%	72	0.8004	0.8217
Lu 6%	126	0.800	0.800

3.5 Photosensitivity (S)

Fabricated PD of undoped Au/NiO/PS and doped Lutetium (Lu_2O_3) at 2% and 6% has been achieved. Photosensitivity (S) by the resistance (R) versus time (t) and with zero bias voltages is shown in Figure 8. The response time is measured by illuminating the PD with (Violet-UV) (365 nm at power 7 W/cm^2). Figure 8 (a) shows the photosensitivity of Au/NiO/PS at an etching current of 15 mA and an etching time of 20 min. The sample was sensitive to light and provided a photosensitivity of 66%, which can be attributed to high porosity, low defect, and high photo active surface areas of the detector. The rise time is achieved to be 0.800 s while the recovery time is discerned to be 0.8000s. Figures 8(b) and 8(c) show the repetitive switching of the Violet-UV for the fabricated PD type Au/NiO:Lu_2O_3/PS at 2% and 6%. Table 3 shows the photosensitivity, rise time, and recovery time. Notably, the doping of rare earth elements leads to the PD improvement, which can be attributed to the increasing lutetium concentration and photosensitivity.

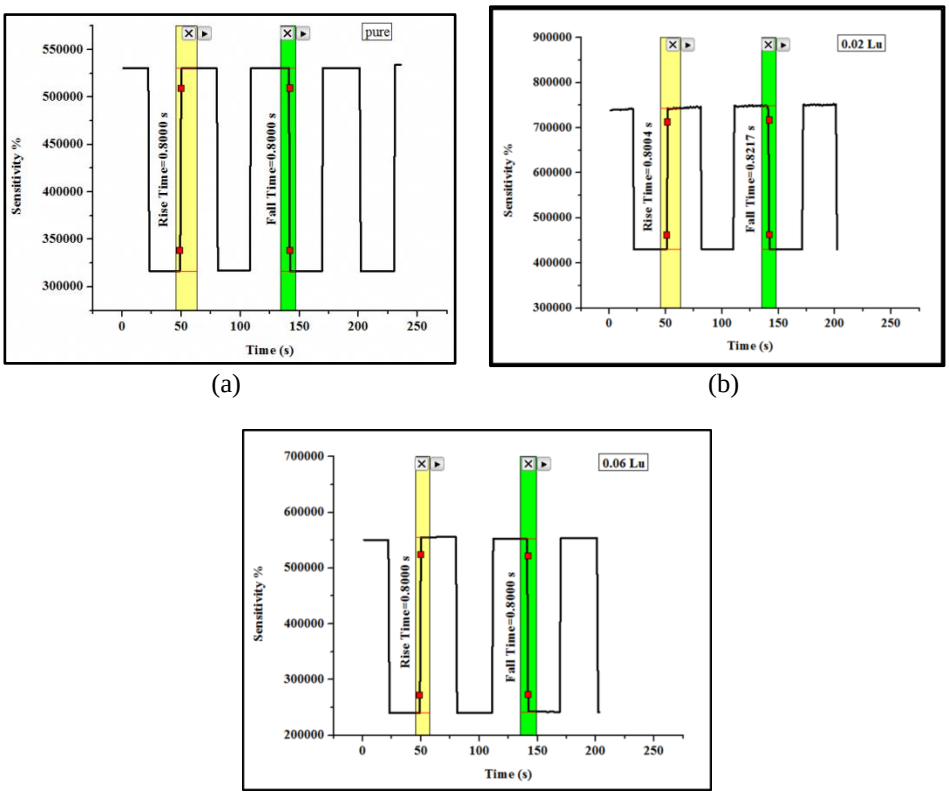

Fig. 8. Repetitive switching of the Au/NiO/PS with doping Lu_2O_3 PDs under (Violet-UV) 400 nm (a) Au/NiO/PS, (b) Au/NiO:Lu_2O_3/PS at 2%, and (c) Au/NiO:Lu_2O_3/PS at 6%

4. Conclusions

The effects of doping ratio Lu_2O_3 on the performance of NiO/PS to fabricated MSM-PD are examined. The results of structure, morphological, and optical properties have been achieved. The XRD pattern of NiO/PS demonstrates that increasing the doping ratio leads to broadening in diffraction peaks, thereby indicating the formation of nanostructure shapes. FESEM image shows that the surface became more homogeneous, spherical, and condensed particle when the doping ratio increased. The energy band gap shifted toward high energy (red shift), thereby resulting in the reduction of grain size. For fabricated Au/NiO:Lu_2O_3/PS, we achieved a good and rapid response, as well as quick recovery time. The electric properties of PD provided good rectifying and ideality factor.

References

[1] M. V. Kumar, S. Muthulakshmi, A. A.Paulfrit, J. Pandiarajan, N.Jeyakumaran, N. Prithivikumaran, Int. J.Chem Tech. Res., **6**(13), 5174 (2014).
[2] J. Arakaki, R. Reyes, M. Horn, W. Estrada, Solar Energy Materials and Solar Cells. **37**(1), 33 (1996).
[3] A. I. Hassan, K. S. Khashan, J. A. Saimon, Eng. &Tech. J. **33**(1), 52 (2015).
[4] D. S. Jbaier, J. A. Simon, K. S. KhashanEng. &Tech. J. **33**(5), 951 (2015).
[5] A. F.Saleh, IJAIEM. **2**(1), 16 (2013).
[6] M. Guziewicz, W. Jung, J. Grochowski, M. Borysiewicz, K. Golaszewska, R. Kruszkaa, A. Baranska, A. Piotrowska, B. S. Witkowskib, J. Z. Domagala, M. Gryzinski, K. Tyminska A. Stonert, Acta Physica Polonica A. **120**(6A), 69 (2011).
[7] M. Guziewics, J. Grochowski,M. Borysiewicz, E .Aminska, J.Domagala,W. Rzodkiewicz,

B. Witkowski, K. Golaszewska, R.Kruszka, M.Ekielski, A. Piotrowski, OpticaApplicata. **XLI**(2), 431 (2011).
[8] A. S. Devasthali, S. G. Kandalkar, IOSR-JCE. **17,** 47 (2015).
[9] D. Wang, R. Xu, X. Wang, Y. Li, Nanotechnology. **17**(4), 979 (2006).
[10] K.Arshak, O. Korostaynska, F. Fahim, Sensors. **3**(6), 176 (2003).
[11] A. J. Hassan, J. Modern Phys. **5**(18), 2184 (2014).
[12] Y. Zhaoa, H. Wangb, C. Wua, Z.F. Shia, F.B. Gaoa, W.C. Lia, G.G. Wua, B.L. Zhanga, G.T. Dua, Vacuum., 10314 (2014).
[13] B. M. Abu-Zied, Salem M. Bawaked, Samia A. Kosa, Wilhelm Schwieger, Catalysts. **6**(70), 1 (2016) .
[14] A. K.Srivastava, S.Thota, J.Kumar J. Nanoscience and Nanotechnology. **8**(8), 4111 (2008).
[15] S. P.Jahromi, N. M. Huang, A. Kamalianfar, H. N.Lim, M. R.Muhamad, R. Yousefi, J. Nanomaterials. **2012**, 1 (2012) .
[16] H. S. TareqEng. &Tech. J. **3**(32) 444 (2014).
[17] A. Largeanu, G.O.Pompilian, D.G.Galusca, M. Ago, S. Gurlui, U.P.B. Sci. Bull. **73**(3), 195 (2011).
[18] B. E. B. Al-Jumaili , Z. A. Talib, A.Ramizy, N. M. Ahmed, L. Y. Josephine, S. B. Paiman, I. B. Muhd, S.A. Abdulateef, J. Nanomaterials. **2016**(3), 1 (2016).
[19] I.M. Ibrahim, E. T. Abdullah, Y. A. AL Shaabani, A. Ramizy, J. Optoelectron. Adv. M. **16**(3-4), 476 (2014).
[20] Sta, M. Jlassi, M. Kandyla, M. Hajji, P. Koralli, R. Allagui, M. Kompitsas, H. Ezzaouia, J. Alloys and Compounds. **626**(87), 87 (2015).
[21] A. S. Ibraheam, Y. Al-Douri, A. S. Mohammed, D. Prakash, U. Hashim, K. D. Verma, Int. J. Electrochem. Sci. **10**(12), 9863 (2015).
[22] I. K.jassim, J. M. Rzaij, I. M. Ali, I. M. Ibrahim, Global. J. engineering science and searches. **3**(1), 26 (2016).
[23] A. Karpinski, N. Ouldhamadouche, A. Ferrec, L. Cattin, M. R. Plouet, L. Brohan, M. A. Djouadi, P. Y. Jouan, Thin Solid Films. **519**(17), 5767 (2011).
[24] F. E.Kruis, H.Fissan, A.Peled, J. Aerosol Sci **29**(5/6), 511 (1998).
[25] E. T. Salem, Nanoscience andNanotechnology. **2**(3), 86 (2012).
[26] P. R. Berger, IEEE Potentials. **15**(2), 25 (1996).
[27] D. A. Neamen, "Semiconductors Physics and Devices Basic Principles",McGraw-Hill, New York., 3rd 351-354(1992).
[28] S.Mahalakshmi, K. S.Manja Int. J. Chem. Tech Res. **7**(3), 1460 (2015).